Laser and Particle Beams (2014), *32*, 33–39.

doi:10.1017/S0263034613000815

Non-equilibrium two-dimensional thermal evolutions in target materials irradiated by femtosecond laser pulse

G. AL-MALKAWI AND A. HASSANEIN

Center for Materials under Extreme Environment, School of Nuclear Engineering, Purdue University, West Lafayette, Indiana

(RECEIVED 9 July 2013; ACCEPTED 17 September 2013)

Abstract

Non-equilibrium heat transfer described by a two-step temperature model was developed to study the thermal evolution through target materials irradiated by femtosecond laser pulse. Two-dimensional heat transfer equations were solved numerically. The temperature dependent thermo-physical properties of the electron and the lattice are considered in the model. The Gaussian spatial and temporal distribution of the heat and temperature of the electron and the lattice is presented. The effect of reflectivity, electron — lattice coupling factor, and the spot size was studied using copper targets.

Keywords: Coupling factor; Femtosecond laser; Spot size; Two temperature model; Ultrashort

INTRODUCTION

The study of ultrashort laser pulses (picosecond and femtosecond) is one of the important evolving research fields because of its unique advantage of having high precision material ablation by extreme high-energy intensities with negligible thermal affected zone. This is because of the very short interacting time period, which is less than the time needed to reach the thermal equilibrium. The ultrashort laser pulses interacting with materials is used for many applications such as drilling, welding, cutting, micro-machining, precise processing of highly sensitive materials, surface alloying (Sonntag *et al.*, 2009; Furusawa *et al.*, 2000; Gurevich *et al.*, 2012), and various medical applications such as brain surgery and removing tumor tissue (Oraevsky *et al.*, 1995; Lee *et al.*, 2009). The physics of ultrashort pulses differs from that for the nanosecond or millisecond range pulses because the pulse width is less than the time needed to reach the equilibrium state between the electrons and the phonons. During the irradiation of metals by picosecond or femtosecond laser pulses the electrons absorb the photon energy and then the heating of the metal lattice occurs by the electron-phonon collisions (Sonntag *et al.*, 2009; Ihtesham *et al.*, 2003; Ihtesham and Xianfan, 2007).

The non-equilibrium heat transfer between the electrons and the lattice can be described by a two temperature model which was first proposed by Anisimov *et al.* (1974) In this model, the heat conduction by the lattice was neglected. After that, Qiu and Tien (1993) used the Boltzmann heat equation and developed the hyperbolic two step radiation heating model and was simplified to the parabolic two step model in which the heating, melting, and evaporation of the materials irradiated by short laser pulses have been solved numerically and have a reasonable agreement with experimental results. Then Qiu and Tien (1993) model was modified by Chen and Beraun (2001) dual hyperbolic two step radiation model in which the heat conduction of the lattice was considered, the electron temperature from both models was very close while there was a remarkable difference in the lattice temperature.

The energy equations that describe the non-equilibrium heat transfer in the two step model are given below (Sonntag *et al.*, 2009; Ihtesham *et al.*, 2003; Zhang and Chen, 2007; Lin *et al.*, 2008):

$$C_e \frac{\partial T_e}{\partial t} = \nabla.(K_e \nabla T_e) - G(T_e - T_l) + Q(\vec{r}, t), \quad (1)$$

$$C_l \frac{\partial T_l}{\partial t} = \nabla.(K_l \nabla T_l) + G_{(T_e - T_l)}. \quad (2)$$

Where T is the temperature, t is the time, C is the volumetric specific heat, K is the thermal conductivity, where the subscripts e and l are associated with the electron and lattice, respectively, G is the coupling factor that describes the

Address correspondence and reprint requests to: G. Al-Malkawi, Center for Materials under Extreme Environment, School of Nuclear Engineering, Purdue University, West Lafayette, IN 47907. E-mail: galmalka@purdue.edu

interaction between the electrons and the lattice, Q is the volumetric laser energy deposition rate as a function of space and time. Eq. (1) describes the heat absorbed by electrons, the electronic heat conduction, the transfer of heat between the electrons and the lattice, and the energy distribution of the laser in time and space. The second equation describes the heat transfer through the lattice, heat conduction and the coupling heat with the electron system.

The laser-heating source as a function of space and time can be described by the following expression:

$$Q(x, y, z, t) = I_0(1 - R)I(t)I(x, y, z). \tag{3}$$

Where I_0 is the maximum power density, R is the reflectivity, $I(t)$, and $I(x,y,z)$ are the temporal distribution and the spatial distribution of the power density, respectively.

INPUT AND ASSUMPTIONS

In this work, a two-dimensional model for the solution of the transient heat transfer equations was developed with temperature and phase change dependent thermal properties (density, thermal conductivity, and specific heat) for both the electron and the lattice. The heat conduction term in the lattice energy equation was neglected because of the slow diffusion in the lattice system during the pulse duration. The Gaussian distribution was assumed for both the time (Tan *et al.*, 2009) and the space (Hassanein, 1983) for the heating source. Therefore, the energy transport equations become (Hassanein, 1983):

$$Ce\frac{\partial T_e}{\partial t} = \frac{1}{r}\frac{\partial}{\partial r}\left(K_e\, r\frac{\partial T_e}{\partial r}\right) + \frac{\partial^2 T_e}{\partial z^2} - G(T_e - T_l) + S(r, z, t), \tag{4}$$

$$Cl\frac{\partial T_l}{\partial t} = G(T_e - T_l). \tag{5}$$

Eq. (4) describes the heat transfer in cylindrical coordinate system where r is the radial direction and z is the direction along the depth inside the target, $s(r,z,t)$ is the volumetric energy from the laser and it depends on r, z, and t as follows:

$$S(r, z, t) = I_0(1 - R)\alpha\, I_{surf}(r)I(t)\exp(-\alpha z), \tag{6}$$

$$I_{surf}(r) = \exp\left(-\frac{r^2}{2\sigma^2}\right), \tag{7}$$

$$I(t) = \exp\left(-\frac{(t - t_p)^2}{\tau^2}\right). \tag{8}$$

Where α is the absorption coefficient, I_0 is the maximal power density, tp is the laser pulse width in time, and $\sigma = r_{\text{beam}}/2$ where r_{beam} is the spot radius of the laser beam.

Thermo Physical Properties and Temperature Dependence

In this work, the thermal properties of electron and lattice such as thermal conductivity, density, and heat capacity were assumed to be dependent on temperature, the following equations describe such dependency (Ihtesham *et al.*, 2003; Zhang and Chen, 2007; Lin *et al.*, 2008; Chen *et al.*, 2011; Ren *et al.*, 2011). The thermal conductivity of electron is given by:

$$k_e = \chi\left(\frac{(\mu_e^2 + 0.16)^{\frac{5}{4}}(\mu_e^2 + 0.44)\mu_e^2}{(\mu_e^2 + 0.092)^{\frac{1}{2}}(\mu_e^2 + \eta\mu_l)}\right). \tag{9}$$

Where χ and η are constants, $\mu_e = T_e/T_F$, $\mu_l = T_l/T_F$, and T_F is the Fermi temperature. The specific heat of the electron is usually a linear function of electron temperature, given by

$$C_e = B_e T_e, \tag{10}$$

where $B_e = \pi^2 n_e k_B/2T_F$, n_e is the density of the free electrons, and k_B is the Boltzmann's constant. The lattice specific heat is in the form of (Jovanović *et al.*, 2009; Garg *et al.*, 1993):

$$C_l = a + bT_l + cT_l^2 + dT_l^3. \tag{11}$$

Where a, b, c, and d are constants which depend on the material.

The density of the material have been assumed temperature and phase dependent and it is given by (Garg *et al.*, 1993; Sangwal, 1987):

$$\rho = c_0 + c_1 T_l + c_2 T_l^2 + c_3 T_l^3, \tag{12}$$

where c_0, c_1, c_2, and c_3 are constants that depend on the material and it's phase. Most of the constants in these equations are tabulated in Table 1.

Initial and Boundary Conditions

The initial value of the target temperature is assumed to be the ambient temperature (300 K) as well as the temperature far away from the exposed surface in r direction and also very far from the center in z direction.

$$T(r, z, t = 0) = T_{amb} = 300\,K,$$

$$T(r = \infty, z, t) = T_{amb} = 300\,K,$$

$$T(r, z = \infty, t) = T_{amb} = 300\,K.$$

The adiabatic boundary conditions have been assumed for both sides in r and z directions

$$\frac{dT}{dr} = 0 \quad \text{for } r = 0, \infty,$$

https://doi.org/10.1017/S0263034613000815 Published online by Cambridge University Press

Table 1. *Thermal and optical properties of Cu*

Electron-lattice coupling factor, G	2.5×10^{11} W/cm^3 K	Ren *et al.* (2011)
Reflectivity, R	0.94	Tan *et al.* (2009); Ren *et al.* (2001); Fang *et al.* (2010)
Absorption coefficient, α	7.1×10^5cm^{-1}	Tan *et al.* (2009); Ren *et al.* (2011); Sangwal (1987)
Fermi temperature, T_F	8.12×10^4	Chen *et al.* (2011); Ren *et al.* (2011)
Electronic heat capacity coefficient, B_e	96.6×10^{-6} J/cm^3 K^2	Lin *et al.* (2008); Ren *et al.* (2011)
Constants in K_e equation, χ, η	3.77, 0.139	Chen *et al.* (2011); Ren *et al.* (2011)
Melting temperature, T_m	1357 K	Ren *et al.* (2011)
Molar weight	63.55 g/mol	Ren *et al.* (2011)
Constants in Eq. (11) for solid and liquid respectively: a, b, c, and d	0.343, 0.00013, 0, and 0 0.514, 0, 0, and 0	Hassanein (1996)
Constants in Eq. (12) for solid and liquid respectively: c_0, c_1, c_2, and c_3	9.211, −0.0009375, 0, and 0 7.8, 0, 0, and 0	Hassanein (1996)

$$\frac{dT}{dz} = 0 \quad \text{for } z = 0, \infty.$$

In this paper, the two temperature model was used to predict the thermal response of Cu target with an ambient temperature of 300 K when exposed to ultrashort laser pulse of 100 fs, spot size of 40 μm, and with a total laser energy of 3.5 μJ. Using Eqs. (6), (7), and (8) the maximum power density was calculated to be 1.5×10^{13} W/cm^2.

RESULTS AND DISCUSSION

The calculation for our two-dimensional heat transfer equations was implemented using non-equilibrium heat transfer equations by modifying the A*THERMAL-2 computer code developed by Hassanein (1996). The finite difference methods were used to calculate both the electron temperature and the lattice temperature. For the 100 fs laser pulse with 40 μm spot size the time step was 0.5 fs up to 100 fs and then increased to 5 fs to the end of the run time. The mesh size in r direction was 0.5 μm and it was changing in z direction to speed up the calculations but maintain the accuracy. The results of the calculated temperatures of lattice and electron and their distribution in space and time as well as the impact of laser spot size, coupling factor, and the material reflectivity are shown and discussed below.

Electron and Lattice Temperature Evaluation

The temporal temperature distribution at the center of the laser beam for both the electron and the lattice is shown in Figure 1, the electron temperature increases very fast within few femtoseconds and reaches to about 11700 K while the lattice temperature increases very slow, at this stage the electrons absorb the photons from the laser and their temperature remains constant to the end of the pulse duration as shown in the upper part of this figure. Then the electrons transfer the absorbed energy to other electrons as well as through the coupling with the phonons, so the temperature of electrons decreases while the lattice temperature increases as shown. However, the decreasing in the electron temperature

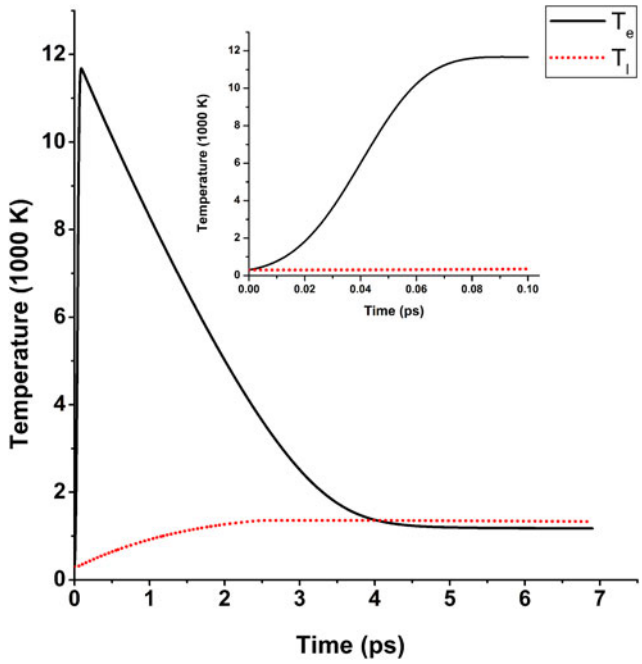

Fig. 1. (Color online) Electron and lattice temperatures of Cu target at the center heated by laser pulse with pulse width of 100 fs, I_0 of 1.5×10^{13} W/cm^2, and spot radius of 20 μm. The upper part is the amplification of the same figure up to 100 fs.

is much faster than the increasing in the lattice temperature because the rate of electron-electron interaction is higher than the rate of electron phonon interactions (Lee *et al.*, 2011). At about 4.8 picoseconds the system reaches thermal equilibrium with temperature about 1330 K.

The equilibrium distribution of the lattice temperature at the surface as a function of r is shown in Figure 2, the temperature has its maximum value at the center of the laser beam ($r = 0$) since the maximum power density of the laser is at the center and according to Eq. (7) the temperature decreases gradually until it reaches 300 K which is the assumed initial temperature at about 34 μm.

Figure 3 shows the temporal and spatial distribution of the electron temperature at the surface. At fixed location the electron temperature increases suddenly until it reaches the

https://doi.org/10.1017/S0263034613000815 Published online by Cambridge University Press

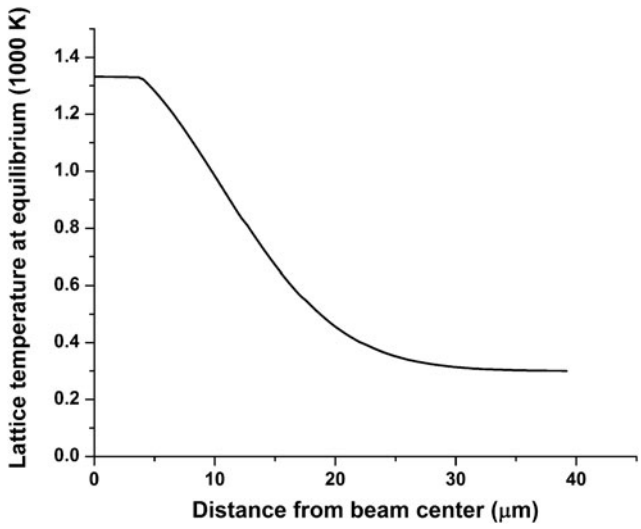

Fig. 2. Lattice equilibrium temperature at the surface as a function of r heated by laser pulse with pulse width of 100 fs, I_0 of 1.5×10^{13} W/cm^2, and spot radius of 20 μm.

maximum value then it decreases gradually until reaching the thermal equilibrium. Figure 3 was extended up to 100 fs which is the value of pulse duration as shown in Figure 4. It can be seen that when the electron temperature reaches its maximum value it remains constant to the end of the pulse width before the decrease in temperature takes place as a result of the electron-phonon coupling. On the other hand, for fixed time the electrons have their maximum

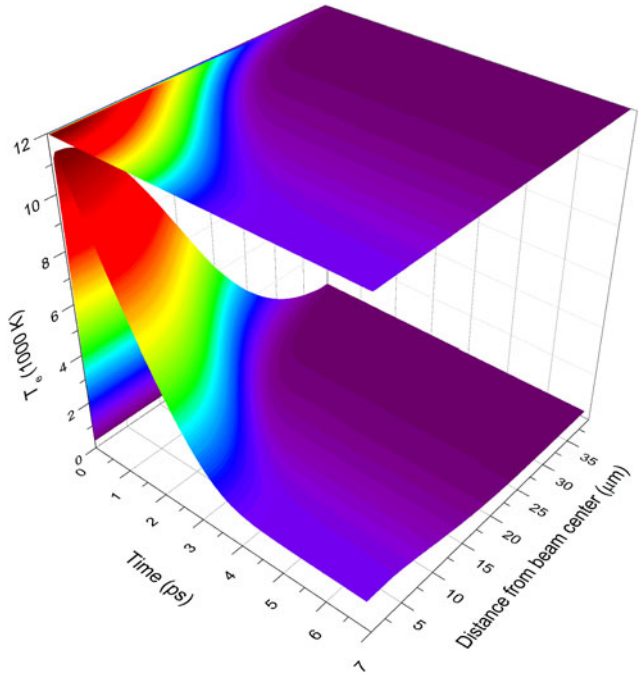

Fig. 3. (Color online) Two-dimensional temporal distribution of the electron temperature at the surface as a function of r irradiated by laser pulse with pulse width of 100 fs, I_0 of 1.5×10^{13} W/cm^2, and spot radius of 20 μm.

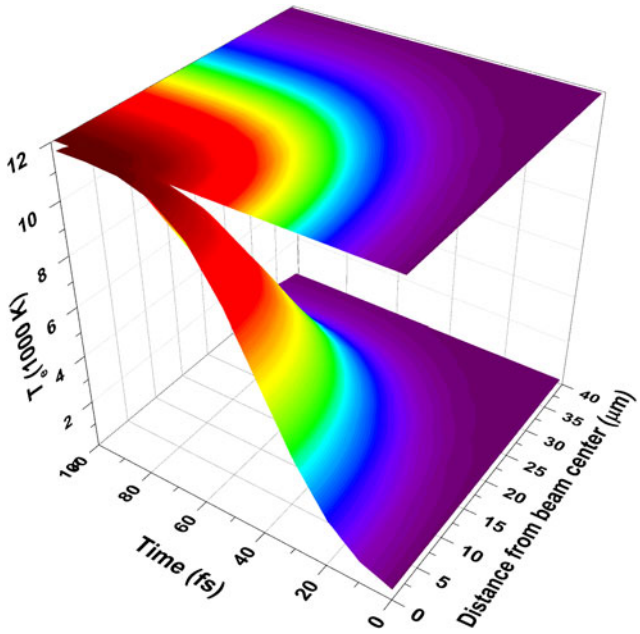

Fig. 4. (Color online) Two-dimensional temporal distribution of the electron temperature at the surface up to 100 fs as a function of r irradiated by laser pulse with pulse width of 100 fs, I_0 of 1.5×10^{13} W/cm^2, and spot radius of 20 μm.

value at the center then decreases with r due to the Gaussian distribution of the power density.

The temporal and spatial distribution of the lattice temperature at the surface is shown in Figure 5 for fixed location the temperature increases with low rate compared to electrons until reaching the thermal equilibrium and for fixed time the temperature decreases far away from the center as discussed above.

The electron and lattice temperature distribution in z direction at the center as a function of time is shown in Figures 6 and 7. The temperature at the center is the maximum and then decreases along with the depth exponentially according to the absorption in z direction as in Eq. (6). The energy needs longer time to be absorbed inside the material. The behavior of the temporal distribution for both electron and lattice at any point along with depth is the same as discussed before.

Parametric Study

The impact of the spot size of the laser beam on the thermal response in the interacting Cu is shown in Figure 8. As the spot size increases the equilibrium temperature decreases because at the fixed total energy the smaller spot size causes higher power density and more heat is deposited at the surface leading to higher temperature. A 40% reduction in the temperature at equilibrium was observed when the spot size increased by 25%. For the spot size of 40 μm using Eqs. (6), (7), and (8), the maximal power density is 1.5×10^{13} W/cm^2 and the thermal equilibrium temperature is

https://doi.org/10.1017/S0263034613000815 Published online by Cambridge University Press

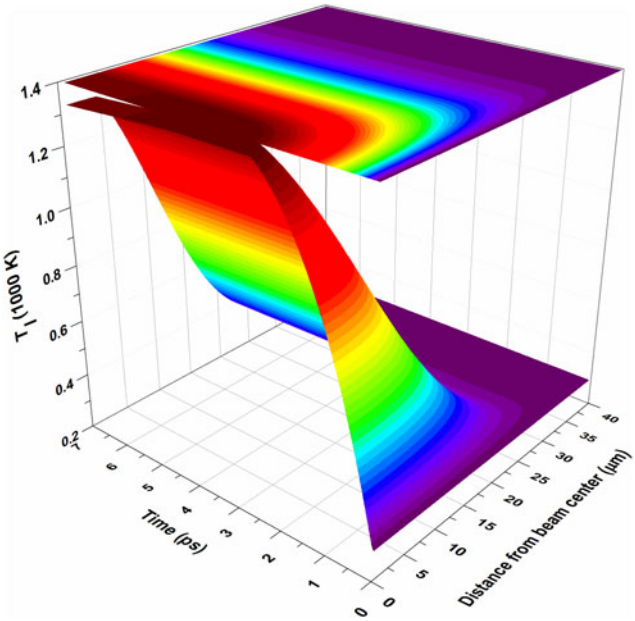

Fig. 5. (Color online) Two-dimensional temporal distribution of the lattice temperature at the surface as a function of r irradiated by laser pulse with pulse width of 100 fs, I_0 of 1.5×10^{13} W/cm^2, and spot radius of 20 μm.

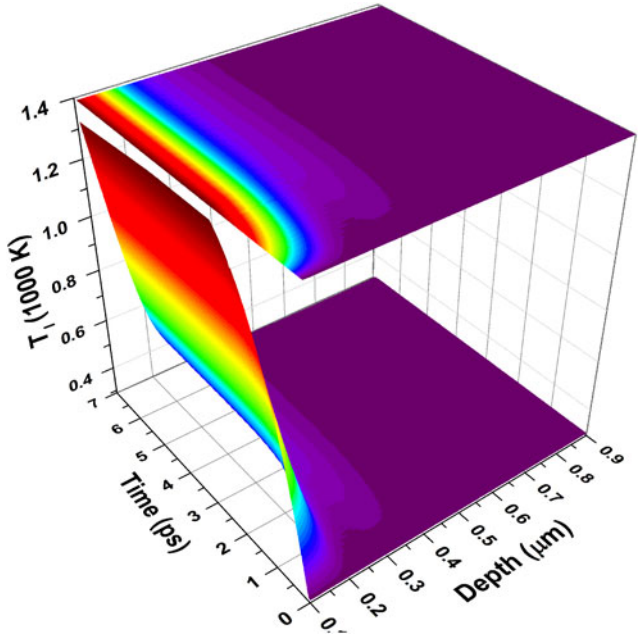

Fig. 7. (Color online) Two-dimensional temporal distribution of the lattice temperature at the center as a function of z irradiated by laser pulse with pulse width of 100 fs, I_0 of 1.5×10^{13} W/cm^2, and spot radius of 20 μm.

about 1330 K whereas for spot size of 50 μm the maximum power density is 8.8×10^{12} W/cm^2 and the equilibrium temperature is only 800 K. On the other hand, smaller spot size causes less heat dissipated in r direction.

Figure 9 shows the impact of the electron-phonon coupling factor. When the value of the coupling factor is 2.5×10^{11} W/cm^3 K the thermal equilibrium between the electron and lattice occurs at about 4.8 ps whereas when its value is 5×10^{11} W/cm^3 K the equilibrium occurs at about 2.6 ps because the higher value of coupling factor increases the rate of the electron phonon interaction such that the thermal equilibrium occurs earlier. Therefore, doubling the coupling factor resulted in reducing the equilibrium time by a factor of 1.8.

The final parameter studied was surface laser reflectivity, which is shown in Figure 10. For the Cu reflectivity of 0.94, the maximum electron temperature is about 11700 and the equilibrium lattice temperature is 1330 K. Whereas for a reflectivity of 0.85 the maximum electron temperature is about 18500 K

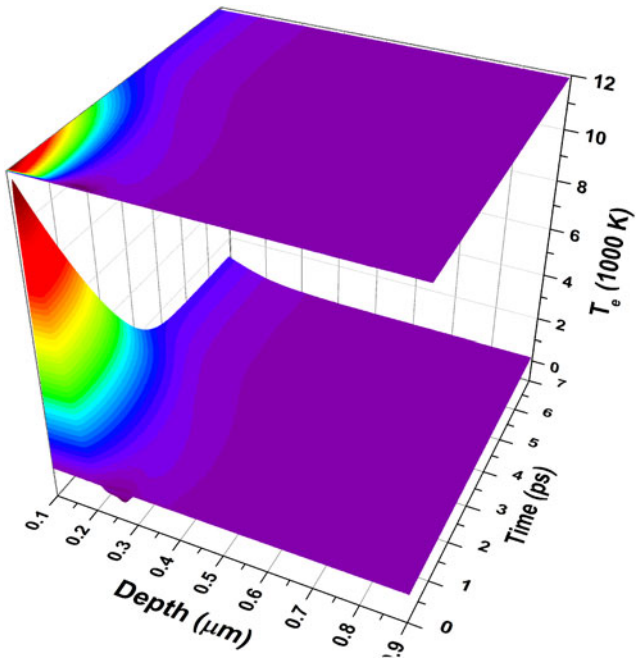

Fig. 6. (Color online) Two-dimensional temporal distribution of the electron temperature at the center as a function of z irradiated by laser pulse with pulse width of 100 fs, I_0 of 1.5×10^{13} W/cm^2, and spot radius of 20 μm.

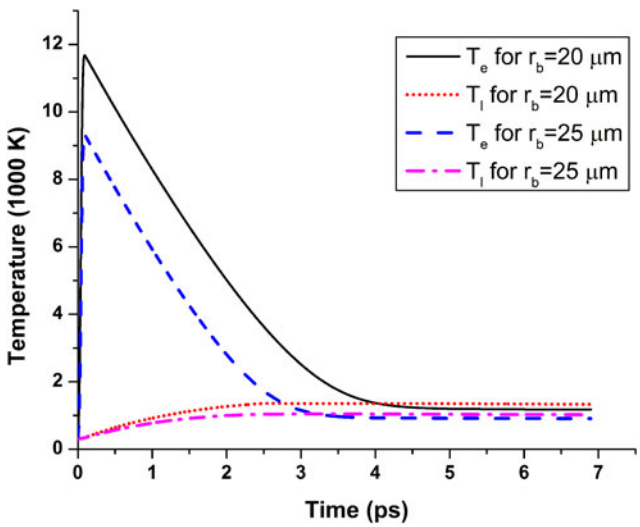

Fig. 8. (Color online) Electron and lattice temperatures at the center irradiated by laser pulse with pulse width of 100 fs, at different values of spot size.

https://doi.org/10.1017/S0263034613000815 Published online by Cambridge University Press

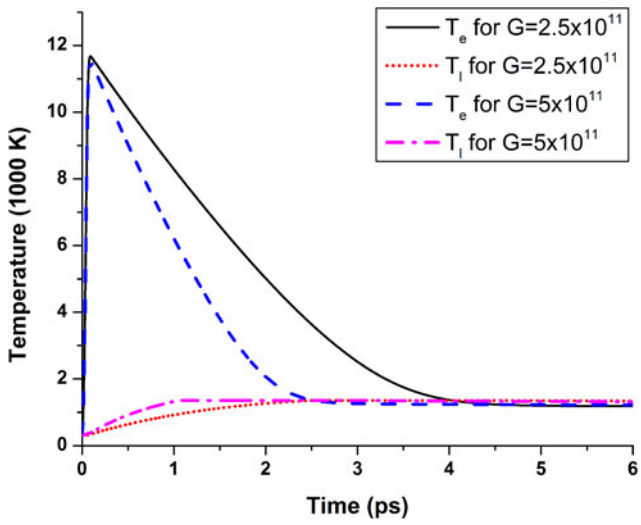

Fig. 9. (Color online) Electron and lattice temperatures at the center irradiated by laser pulse with pulse width of 100 fs, I_0 of 1.5×10^{13} W/cm^2, and spot radius of 20 μm at different values of electron-phonon coupling factor.

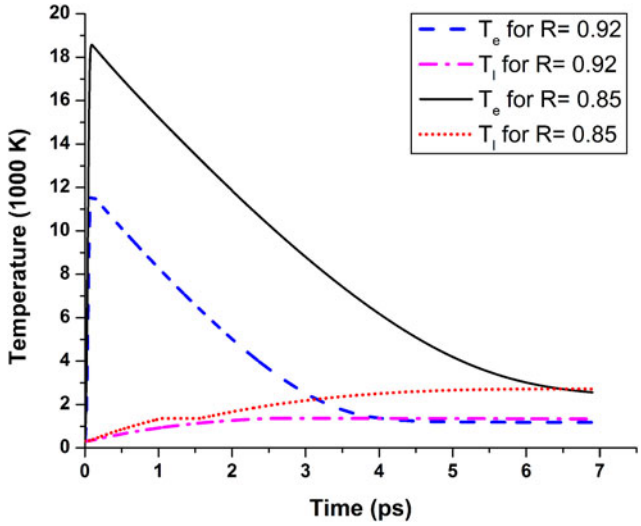

Fig. 10. (Color online) Electron and lattice temperatures at the center irradiated by laser pulse with pulse width of 100 fs, I_0 of 1.5×10^{13} W/cm^2, and spot radius of 20 μm at different values of reflectivity.

and the equilibrium temperature is about 2700 K, this is because as the reflectivity increases more photons from the input laser are reflected which leads to less laser power deposited on the surface. In this case, a 10% decrease in target surface reflectivity increased the equilibrium temperature by a factor of 2. This is in contrast to nanosecond laser pulses where the reflected laser light will be absorbed in the evolving plasma of the target materials and additionally heating such plasma that can further contribute to erosion of target materials.

CONCLUSION

In this work, a two-step temperature model was developed and used to study the non-equilibrium thermal two-dimensional heat distribution when Cu target is irradiated by femtosecond laser pulse with temperature dependent thermal properties. Gaussian temporal and spatial distributions of laser power density were assumed in our simulation. The predicted behavior of the temperature distribution of the electron and the lattice as a function of t, r, and z was explained by the physics of the heat exchange mechanisms among electrons, photons, and lattice atoms. The electrons initially absorb the laser photons and their temperature increase rapidly to maximum value then remains constant to the end of the femtosecond pulse. Then the heat is transferred to other electrons and phonons such that the electron temperature decreases and lattice temperature increases till reaching the thermal equilibrium. The impact of the spot size of the femtosecond laser beam was also studied and the larger spot size for a fixed total energy leads to smaller maximum power density so less heat deposited to the material and finally lower equilibrium temperature. The coupling factor has an impact on the rate of interaction between the electrons and the lattice, higher values causes higher rate of interaction and faster thermal equilibrium. Finally, the effect of laser reflectivity was studied and that higher value of reflectivity leads to high rate of photons reflection and less absorption of the energy in the target. This process should also be function of target condition during irradiation, as reflectivity changes as the state of the material changes from solid to liquid to gas/vapor phases. This will be studied in future work.

ACKNOWLEDGEMENT

This work is partially supported by the US Department of Energy, Office of Fusion Energy Sciences.

REFERENCES

Anisimov, S.I., Kapeliovich, B.L. & Perel'man, T.L. (1974). Electron emission from metal surfaces exposed to ultrashort laser pulses. *Sov. Phys.-JETP* **39**, 375.

Chen, J.E.B.J.K. (2001). Numerical study of ultrashort laser pulse interactions with metal films. *Numerical Heat Transf. A* **40**, 1.

Chen, A.M., Jiang, Y.F., Sui, L.Z., Ding, D.J., Liu, H. & Jin, M.X. (2011). Thermal behavior of thin metal films irradiated by shaped femtosecond pulse sequences laser. *Opt. Commun.* **284**, 2192.

Fang, R., Zhang, D., Wei, H., Li, Z., Yang, F. & Gao, Y. (2010). Improved two-temperature model and its application in femtosecond laser ablation of metal target. *Laser Part. Beams* **28**, 157.

Furusawa, K., Takahashi, K., Cho, S.-H., Kumagai, H., Midorikawa, K. & Obara, M. (2000). Femtosecond laser micromachining of TiO_2 crystal surface for robust optical catalyst. *J. Appl. Phys.* **87**, 1604.

Garg, S.K., Banipal, T.S. & Ahluwalia, J.C. (1993). Heat capacities and densities of liquid o-xylene, m-xylene, p-xylene, and ethylbenzene, at temperatures from 318.15 K to 373.15 K and at pressures up to 10 MPa. *J. Chem. Thermodyn.* **25**, 57.

https://doi.org/10.1017/S0263034613000815 Published online by Cambridge University Press

Gurevich, E.L., Kittel, S. & Hergenröder, R. (2012). Experimental and numerical study of surface alloying by femtosecond laser radiation. *Appl. Surf. Sci*. **258**, 2576.

Hassanein, A.M. (1983). Modeling the interaction of high power ion or electron beams with solid target materials. Aragonne National laboratory, ANL/FPP/TM-179.

Hassanein, A. (1996). Disruption damage to plasma-facing components from various plasma instabilities. *Fusion Techn*. **30**, 713.

Ihtesham, H., Chowdhury, H. & Xianfan, X. (2003). *Heat transfer in femtosecond laser processing of metal*. *Numerical Heat Transf. A* **44**, 219.

Jovanović, J.D., Knežević-Stevanović, A.B. & Grozdanić, D.K. (2009). An empirical equation for temperature and pressure dependence of liquid heat capacity. *J. Taiwan Institute Chem. Engin*. **40**, 105.

Lee, H., Jeong, Y.-U. & Chan, K.L. (2009). The advent of laser therapies in dermatology and urology: Underlying mechanisms, recent trends and future directions. *J. Opt. Soc. Korea* **13**, 321.

Lee, J.B., Kang, K. & Lee, S.H. (2011). Comparison of Theoretical Models of Electron-Phonon Coupling in Thin Gold Films Irradiated by Femtosecond Pulse Lasers. *Mater. Transact*. **52**, 547.

Lin, Z., Zhigilei, L. & Celli, V. (2008). Electron-phonon coupling and electron heat capacity of metals under conditions of strong electron-phonon nonequilibrium. *Phys. Rev. B* **77** (7).

Oraevsky, A.A., DaSilva, L.B., Feit, M.D., Glinsky, M.E., Mammini, B.M., Paquette, K.L., Perry, M.D., Rubenchik, A.M., Small IV, W. & Stuart, B.C. (1995). Plasma mediated ablation of biological tissues with ultrashort laser pulses. *Proc. SPIE* **2391**, 423.

Qiu, T.Q. & Tien, C.L. (1993). Heat transfer mechanisms during short-pulse laser heating of metals. *J. Heat Transf*. **115**, 835.

Ren, Y., Chen, J.K. & Zhang, Y. (2011). Optical properties and thermal response of copper films induced by ultrashort-pulsed lasers. *J. Appl. Phys*. **110**, 113102.

Sangwal, K. (1987). A new equation for the temperature dependence of density of saturated aqueous solutions of electrolytes. *Cryst. Res. Technol*. **22**, 789.

Sonntag, S., Roth, J., Gaehler, F. & Trebin, H.R. (2009). Femtosecond laser ablation of aluminium. *Appl. Surf. Sci*. **255**, 9742.

Tan, X.-y., Zhang, D.-m., Mao, F., Li, Z.-h., Yi, D.I. & Zhang, X.-z. (2009). Theoretical and experimental study of energy transportation and accumulation in femtosecond laser ablation on metals. *Transact. Nonferrous Metals Soc. China* **19**, 1645.

Zhang, Y. & Chen, J.K. (2007). Melting and resolidification of gold film irradiated by nano- to femtosecond lasers. *Appl. Phys. A* **88**, 289.